

# Weyl's problem: A computational approach

Isaac Bowser,<sup>\*</sup> Ken Kiers,<sup>†</sup> and Erica Mitchell<sup>‡</sup>

*Physics and Engineering Department, Taylor University,  
236 West Reade Ave., Upland, Indiana 46989*

Joshua Kiers<sup>§</sup>

*Department of Mathematics, University of North Carolina at Chapel Hill,  
CB# 3250 Phillips Hall, Chapel Hill, North Carolina 27599-3250*

(Dated: August 13, 2024)

## Abstract

The distribution of eigenvalues of the wave equation in a bounded domain is known as Weyl's problem. We describe several computational projects related to the cumulative state number, defined as the number of states having wavenumber up to a maximum value. This quantity and its derivative, the density of states, have important applications in nuclear physics, degenerate Fermi gases, blackbody radiation, Bose-Einstein condensation and the Casimir effect. Weyl's theorem states that, in the limit of large wavenumbers, the cumulative state number depends only on the volume of the bounding domain and not on its shape. Corrections to this behavior are well known and depend on the surface area of the bounding domain, its curvature and other features. We describe several projects that allow readers to investigate this dependence for three bounding domains – a rectangular box, a sphere, and a circular cylinder. Quasi-one- and two-dimensional systems can be analyzed by considering various limits. The projects have applications in statistical mechanics, but can also be integrated into quantum mechanics, nuclear physics, or computational physics courses.

## I. INTRODUCTION

From the late 1800s to the early 1970s, Weyl and many others studied the distribution of eigenvalues of the wave equation,

$$-\nabla^2\psi = k^2\psi, \tag{1}$$

inside a finite domain such as a sphere, cube, or other shapes. Many physical systems are described by Eq. (1), differing only in the definition of the wavenumber  $k$  and in the boundary conditions. The cumulative state number (or mode number or integrated density of states),  $N(k)$ , is the number of distinct states at or below some value of  $k$ ; the derivative of  $N(k)$  is the density of states. Knowledge of the functional form of  $N(k)$  and/or the density of states is of great importance in studies of blackbody radiation, the Casimir effect, acoustics and elasticity, Bose-Einstein condensation, nuclear physics and degenerate Fermi gases. Reference 1 provides an excellent overview of this field, including many details and an extensive review of the literature up to the early 1970s.

According to Ref. 1, Pockels<sup>2</sup> was the first to count the eigenvalues of Eq. (1), with subsequent and related work done by Rayleigh, Lorentz, Reudler, Weyl, and others.<sup>1,3,4</sup> Of particular importance is the large  $k$  behavior of  $N(k)$ , which was shown to be independent of the shape of the bounding domain and to depend only on its volume, a result now known as Weyl's theorem.<sup>4</sup> Corrections to the infinite volume result depend on the surface area of the bounding domain, its curvature, and on other geometrical features. There is an extensive literature on the importance of surface and shape effects in various areas of physics (see Ref. 1, p. 11).

In this paper we study Weyl's problem in the context of a rectangular parallelepiped, a sphere and a circular cylinder, which were chosen because the eigenvalues are well known and may be computed straightforwardly. For the rectangular and cylindrical cases we can analyze quasi-one- and two-dimensional structures, which are of theoretical and experimental interest.

Our focus is on comparing exact (discrete) results for  $N(k)$  with the approximate asymptotic result. Historically, there has been an interesting interplay between computational and analytical approaches to the problem.<sup>5</sup>

For the bounding domains that we consider, the eigenstates may be labeled by triplets of integers, and the states contributing to  $N(k)$  for a particular value of  $k$  may be represented by points on a three-dimensional lattice. These points are bounded by a surface in this space, and calculation of  $N(k)$  reduces to summing the points within this bounding surface. Students will likely be familiar with the cubic bounding domain, for which the bounding surface in the complementary space is one eighth of a sphere. For a general rectangular domain, the bounding surface becomes one eighth of an ellipsoid.

For large  $k$  it is appropriate to treat  $k$  as a continuous variable and to replace sums over points on a lattice by integrals. Textbook derivations of  $N(k)$  and related quantities usually follow this approach and take the bounding domain to be a cube. In this work we show how we can follow this approach for all three of the bounding domains we consider, and derive both the leading volume term in the asymptotic expansion as well as the (subleading) surface area terms. The spherical and cylindrical cases are more involved and are treated in the appendices.

This paper includes several computational projects to help students verify and analyze various topics related to Weyl's problem. We include algorithms and pseudocode that encourage students to approach the problem from a geometrical perspective. Although as physicists we are generally adept at switching between sums and integrals, our students may perceive this as a sleight of hand. The computations we describe will improve students' computational abilities, while simultaneously helping them to develop their intuition and ability to understand the limitations of the simplifying assumptions. For example, one might wonder about the applicability of the continuum approximation when the bounding domain is quasi-one- or two-dimensional. In this case, the wavenumber is much more sensitive to the quantum numbers associated with the small dimensions, and it is difficult to imagine that approximating a sum by an integral is justified in this case.<sup>6</sup> We shall see that the approach to asymptopia is very slow for systems that are quasi-one- or two-dimensional. And yet such systems do eventually approach the asymptotic limiting behavior required by Weyl's theorem.

Although our focus is almost exclusively on Weyl's problem, the literature gives many examples of possible applications. Molina<sup>7</sup> and Gutiérrez and Yáñez<sup>8</sup> consider thermodynamic quantities related to an ideal gas in a finite-sized container, focusing on effects due to the shape of the container, such as the ratio of the surface area to the volume.

References 9 and 10 analyze Bose-Einstein condensation in a finite-sized one-dimensional box and in spherically symmetric traps, respectively. The latter includes a discussion of a quasi-two-dimensional “bubble trap,” as well as references to relevant experimental work in the context of cold gases.<sup>10</sup> Price and Swendson use numerical computation as a means for teaching topics related to ideal quantum gases and describe various projects that allow students to compute the chemical potential and related quantities.<sup>11</sup> Mulhall and Moelter calculate  $N(k)$ , use it to compute an approximate density of states for a rectangular box and a sphere, and then extend the results to a system of non-interacting bosons.<sup>12</sup> Balian and Bloch analyze the oscillations of the smoothed density of eigenvalues, noting their important application in nuclear physics.<sup>13</sup> Cottingham and Greenwood discuss the integrated density of states in a nuclear context, including a plot comparing the exact (discrete) version to an asymptotic expression which includes the leading volume and subleading surface terms.<sup>15</sup> We also note connections to the Casimir effect<sup>16</sup> and to the growing body of literature on nanostructures.<sup>18</sup>

The remainder of this paper is organized as follows. In Sec. II we define the cumulative state number,  $N(k)$ , and give the averaged asymptotic expressions to which our numerical results will be compared. We give the eigenvalues for the rectangular parallelepiped, the sphere and the circular cylinder and show how the states contributing to  $N(k)$  can be visualized as points on a lattice. We also derive the leading and first subleading contributions to the asymptotic expressions for the rectangular case. In Sec. III we describe several projects and problems. Section IV contains some discussion and concluding remarks. Appendix A gives expressions for the wave functions. In Appendix B we describe algorithms that can be used for the various projects, including an efficient algorithm for the spherical case and pseudocode. In Appendix C we derive the leading and first subleading contributions to  $\overline{N}(k)$  for the spherical and cylindrical cases.

## II. DISTRIBUTION OF EIGENVALUES FOR THREE GEOMETRICAL SHAPES

Consider Schrödinger’s equation for a particle that is free within some bounded domain,

$$-\frac{\hbar^2}{2\mu}\nabla^2\psi = \epsilon\psi, \quad (2)$$

where  $\epsilon$  is the energy of the particle and  $\mu$  is its mass. Defining the wavenumber as

$$k = \sqrt{\frac{2\mu\epsilon}{\hbar^2}} \quad (3)$$

immediately gives Eq. (1). We consider a rectangular parallelepiped with linear dimensions  $L_x$ ,  $L_y$  and  $L_z$  (in the  $x$ ,  $y$  and  $z$  directions, respectively), a sphere of radius  $a$  and a circular cylinder of height  $L$  (in the  $z$  direction) and radius  $a$ . The particle is free inside the box in each case. At the boundary of the box we assume Dirichlet boundary conditions; that is,  $\psi = 0$  at the boundary. Other boundary conditions may also be assumed and are appropriate for problems such as an electromagnetic wave inside of a cavity, or sound waves inside an acoustic resonator.<sup>1</sup>

By solving Eq. (1) with the boundary conditions we find that the energy eigenvalues and hence wavenumbers are quantized (see Appendix A); that is, the wavenumbers form an (infinite) discrete set. The wavenumbers may be labeled by triplets of integers and thus may be thought to be on a three-dimensional lattice. We denote the eigenvalues by  $k_{\vec{n}}$ , where  $\vec{n}$  represents the triplet of integers labeling the state. The cumulative state number,  $N(k)$ , counts the number of distinct states for which  $k_{\vec{n}} \leq k$ . That is,<sup>19</sup>

$$N(k) = \sum_{k_{\vec{n}} \leq k} 1. \quad (4)$$

Weyl showed that, in the limit of large  $k$ ,  $N(k)$  is approximately proportional to the volume,  $V$ , of the domain,<sup>4</sup>

$$N(k) \sim \frac{Vk^3}{6\pi^2} + \dots, \quad (5)$$

independent of the shape of the domain. This result is sometimes referred to as Weyl's theorem. For many applications in statistical mechanics it is sufficient to keep only the first term in Eq. (5). Thus, for example, the Fermi energy is<sup>20</sup>

$$\epsilon_F = \frac{\hbar^2 k^2}{2\mu} \simeq \frac{\hbar^2}{2\mu} \left( \frac{3\pi^2 N_f}{V} \right)^{2/3}, \quad (6)$$

where the number of fermions,  $N_f$ , is twice  $N(k)$ , because two spin-1/2 fermions can be in each of the states. Equation (6) holds only for large  $k$ ; for smaller  $k$  we must be careful (see Ref. 11 for a discussion of the case  $N_f = 1$ ). The density of states, which is the number of

	$M$	$J$
Rectangular Parallelepiped	$\frac{3\pi}{2} (L_x + L_y + L_z)$	$-64\pi$
Sphere	$4\pi a$	$0$
Circular Cylinder	$\frac{\pi}{2} (2L + 3\pi a)$	$2\pi \left( \frac{L}{a} - \frac{64}{3} \right)$

TABLE I. The constants  $M$  and  $J$  in Eq. (8) for the rectangular parallelepiped, sphere and circular cylinder.<sup>1,8,23</sup>

single-particle states per unit energy, is<sup>21</sup>

$$g(\epsilon) = \frac{dN}{dk} \frac{dk}{d\epsilon} \simeq \frac{V\mu^{3/2}}{\sqrt{2}\pi^2\hbar^3} \epsilon^{1/2}, \quad (7)$$

where we have used Eq. (3).

Many corrections to Eq. (5) have been computed over the years. As noted in Ref. 1, the difference between  $N(k)$  and its asymptotic approximations exhibits fluctuations that disguise the geometric nature of the approximation. To gain insight into the structure of the cumulative state number, it is necessary to perform some averaging over the eigenvalues. This averaging can also be interpreted physically because, for example, we do not have measuring devices that can measure with perfect accuracy, and the walls of bounding domains are not perfectly rigid or smooth.<sup>1</sup> In practice, these effects lead to a natural sort of averaging. There is an extensive literature on how to average over the eigenvalues.<sup>1</sup> Having performed the averaging in an appropriate manner, we can make rigorous statements about the behavior of  $\overline{N}(k)$  as a function of  $k$ . The averaged asymptotic expression for  $\overline{N}(k)$  for the cases we consider is given by<sup>1,8,22,23</sup>

$$\overline{N}(k) \sim \frac{Vk^3}{6\pi^2} - \frac{Sk^2}{16\pi} + \frac{Mk}{6\pi^2} + \frac{J}{512\pi} + \dots \quad (8)$$

for Dirichlet boundary conditions;  $S$  is the surface area of the bounding domain. For smooth boundaries, the quantities  $M$  and  $J$  may be expressed as surface integrals that depend on the radii of curvature of the domain.<sup>24</sup> Expressions for the rectangular parallelepiped, sphere and cylinder are found in Table I.

In the following we give expressions for the eigenvalues for the three geometrical domains and the cumulative state number  $N(k)$ . We also give a quasi-rigorous derivation of the first

two terms in Eq. (8) for the rectangular parallelepiped. The derivations for the spherical and cylindrical cases are given in Appendix C. In principle we can also calculate the density of states numerically. The density of states is a sum of delta functions corresponding to the slopes of the steps in  $N(k)$  (see Ref. 22), but we can smooth the distribution in various ways.<sup>1,12,22</sup> Because the density of states involves a derivative, it is a noisier quantity,<sup>12</sup> and thus we will consider only the cumulative state number.

### A. Rectangular parallelepiped

The eigenvalues for the rectangular parallelepiped may be written as

$$k_{n_x n_y n_z}^2 = \pi^2 \left( \frac{n_x^2}{L_x^2} + \frac{n_y^2}{L_y^2} + \frac{n_z^2}{L_z^2} \right) \quad (9)$$

(see Appendix A 1), so that  $N(k)$  sums up the states satisfying

$$\pi^2 \left( \frac{n_x^2}{L_x^2} + \frac{n_y^2}{L_y^2} + \frac{n_z^2}{L_z^2} \right) \leq k^2, \quad (10)$$

where  $n_x$ ,  $n_y$  and  $n_z$  each independently take on the values 1, 2, 3, ...

Figure 1 shows the states contributing to  $N(k)$  for  $kV^{1/3} = 15\pi$ , with  $L_x = 1.25L_z$  and  $L_y = 1.5L_z$ . The inequality in Eq. (10) shows that the bounding surface is an ellipsoid in  $n_x n_y n_z$  space. Let us imagine attempting to count the points. Because the integers  $n_x$ ,  $n_y$  and  $n_z$  are all positive, we first count all of the points inside the entire bounding ellipsoid (including points with  $n_x$ ,  $n_y$  or  $n_z$  equal to zero), and then subtract the points in the  $n_x n_y$ ,  $n_y n_z$  and  $n_x n_z$  planes. Having done so, we will have subtracted the points along each of the axes twice, so they need to be added back in once. Finally, the origin needs to be subtracted out once, and the result divided by 8. The number of points can thus be written as<sup>25</sup>

$$N_{\text{rect}}(k) = \frac{1}{8} [A_3(k) - A_2^{xy}(k) - A_2^{yz}(k) - A_2^{xz}(k) + A_1^x(k) + A_1^y(k) + A_1^z(k) - 1], \quad (11)$$

where  $A_3$  is the sum of all points inside the ellipsoidal volume,  $A_2^{ij}$  represents the sums bounded by ellipses in the various planes, and  $A_1^i$  represents the sums along the axes.

For  $k \gg 1/L_i$ , the sum represented by  $A_3(k)$  may be approximated by an integral. Because the points in  $\vec{n}$ -space are uniformly spaced (with unit density),  $A_3(k)$  is approximately

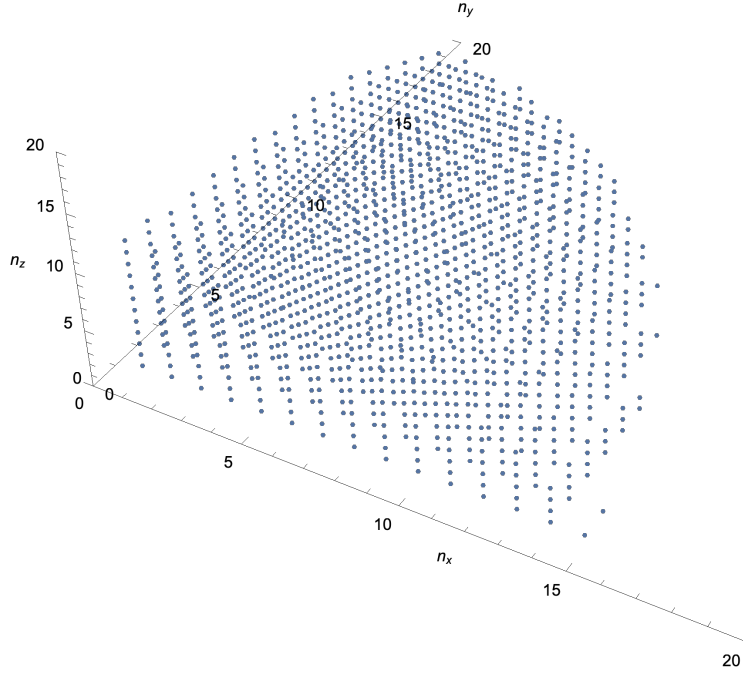


FIG. 1. States contributing to  $N(k)$  for  $kV^{1/3} = 15\pi$  for a rectangular parallelepiped with  $L_x = 1.25L_z$  and  $L_y = 1.5L_z$ .  $N(k)$  is the total number of points in the plot which, in this case, is 1505. Only positive integers  $n_x$ ,  $n_y$  and  $n_z$  are included in the sum.

equal to the volume of the bounding ellipsoid,

$$\frac{4}{3}\pi \left(\frac{kL_x}{\pi}\right) \left(\frac{kL_y}{\pi}\right) \left(\frac{kL_z}{\pi}\right) = 4k^3 L_x L_y L_z / (3\pi^2), \quad (12)$$

or

$$A_3(k) = \frac{4Vk^3}{3\pi^2} + P_3(k), \quad (13)$$

where  $V = L_x L_y L_z$  and  $P_3(k)$  is the error incurred by approximating the sum of lattice points by an integral.<sup>1</sup> We can proceed similarly for  $A_2^{ij}$  by approximating the sums in the various planes by the areas of the corresponding ellipses to find

$$A_2^{ij}(k) = \frac{1}{\pi} L_i L_j k^2 + P_2^{ij}(k). \quad (14)$$

If we substitute Eqs. (13) and (14) into Eq. (11), drop the remainders and note that  $S = 2(L_x L_y + L_y L_z + L_x L_z)$ , we can reproduce the first two terms in Eq. (8).

Our derivation of the surface area term in Eq. (8) has been heuristic. In particular, we have implicitly assumed that the lattice remainder from the volume term is smaller than



$O(k^2)$ , so that it does not overwhelm our calculation of the surface area term. Reference 1 discusses lattice remainders and the asymptotic expression for  $N$ ; the result that we have derived is accurate when the averaging is done appropriately.

Suppose that instead of doing the volume integral over the entire ellipsoid and then dividing by eight, we had done the volume integral over one eighth of the ellipsoid. This integral would have included contributions from the points on the lattice on each of the planes  $n_x = 0$ ,  $n_y = 0$  and  $n_z = 0$ . The area of each of these contributions is one quarter of the area of the corresponding ellipse represented by  $A_2^{ij}$ . And yet we see that we must subtract one eighth this area, not one fourth. Evidently the one eighth volume integral, with its bounding surfaces precisely at  $n_x = 0$ , etc., effectively captures a number of lattice points equal to one half the surface area of each of these bounding surfaces; this is the amount that must be subtracted. Alternative approaches are to perform the volume integration in one eighth of the space, but starting from  $n_x, n_y, n_z = 1$  (in which case an area integral must be added to the result to correct for the fact that only half the contributions from the bounding surfaces at  $n_x, n_y, n_z = 1$  are included in the volume integral) or to perform the volume integral starting from  $n_x, n_y, n_z = 1/2$  (in which case no area correction needs to be done). All of these approaches yield the same result to order  $k^2$ .

To compare different domain shapes on the same plot, it is convenient to define the following dimensionless variables,

$$\kappa = kV^{1/3} \tag{15}$$

$$\xi_x = L_x/L_z \tag{16}$$

$$\xi_y = L_y/L_z, \tag{17}$$

so that

$$\kappa_{n_x n_y n_z}^2 = \pi^2 \left[ n_x^2 \left( \frac{\xi_y}{\xi_x^2} \right)^{2/3} + n_y^2 \left( \frac{\xi_x}{\xi_y^2} \right)^{2/3} + n_z^2 (\xi_x \xi_y)^{2/3} \right]. \tag{18}$$

We can now write Eq. (8) for the rectangular parallelepiped as

$$\overline{N}_{\text{rect}}(\kappa) \sim \frac{\kappa^3}{6\pi^2} - \kappa^2 f_{\text{rect}}^{(2)}(\xi_x, \xi_y) + \kappa f_{\text{rect}}^{(1)}(\xi_x, \xi_y) - \frac{1}{8} + \dots, \tag{19}$$

where

$$f_{\text{rect}}^{(1)}(\xi_x, \xi_y) = \frac{1}{4\pi} \left[ \left( \frac{\xi_x^2}{\xi_y} \right)^{1/3} + \left( \frac{\xi_y^2}{\xi_x} \right)^{1/3} + \left( \frac{1}{\xi_x \xi_y} \right)^{1/3} \right] \quad (20)$$

$$f_{\text{rect}}^{(2)}(\xi_x, \xi_y) = \frac{1}{8\pi} \left[ (\xi_x \xi_y)^{1/3} + \left( \frac{\xi_x}{\xi_y^2} \right)^{1/3} + \left( \frac{\xi_y}{\xi_x^2} \right)^{1/3} \right]. \quad (21)$$

Equation (19) gives the averaged asymptotic expression to which we can compare our exact (discrete) results. Note that the leading term is independent of the shape of the rectangular box and has the same form for a cube as it does for a quasi-one- or two-dimensional box. The shape dependence only shows up in the subleading terms, which depend on  $\xi_x$  and  $\xi_y$ .

Figure 2 shows  $N(\kappa)$  as a function of  $\kappa$  for two rectangular parallelepipeds. The exact results consist of a series of discrete steps corresponding to the addition of new states at various values of  $\kappa$ . We have derived  $N(\kappa)$  following the algorithm outlined in Appendix B 1, which essentially corresponds to adding up the number of states in a region similar to that shown in Fig. 1.<sup>26</sup> Most textbook derivations of the cumulative state number include only the leading volume term. As is evident from Fig. 2, the volume term in Eq. (19) (proportional to  $\kappa^3$ ) does not give a good estimate for  $N(\kappa)$  for small  $\kappa$ . Inclusion of the negative surface area term (proportional to  $\kappa^2$ ) improves the agreement significantly, but overshoots somewhat. Inclusion of all four terms in Eq. (19) leads to good agreement on average, although the exact result fluctuates about the asymptotic curve. The corrections to the leading term are of order  $\kappa^2$  and become unimportant as  $\kappa \rightarrow \infty$ . We note that the approach to the asymptotic behavior is much slower for the quasi-one-dimensional structure in Fig. 2(b) (that is, the curve is displaced further to the right) than for the cubic structure.

The quasi-one-dimensional case in Fig. 2(b) also exhibits cusps. To understand these, note that the  $n_x^2$  coefficient in Eq. (18) is much smaller than the  $n_y^2$  and  $n_z^2$  coefficients in this case. Thus, between  $\kappa \approx 9$  and  $\kappa \approx 15$ ,  $n_y = n_z = 1$  and  $N = n_x$ . Indeed,  $N(\kappa)$  between  $\kappa \approx 9$  and  $\kappa \approx 15$  is relatively well-described by a continuous curve that depends only on  $n_x$ . For  $\kappa \gtrsim 15$ , states with  $(n_y, n_z) = (1, 2)$  and  $(2, 1)$  also start to contribute to  $N(\kappa)$ , leading to an abrupt change in slope of  $N(\kappa)$ . The quasi-two-dimensional case also exhibits cusps, and the behavior of  $N(\kappa)$  at and between the cusps may similarly be understood by considering quantum numbers associated with the large and small directions to behave quasi-continuously and discretely, respectively. The situation here is reminiscent of

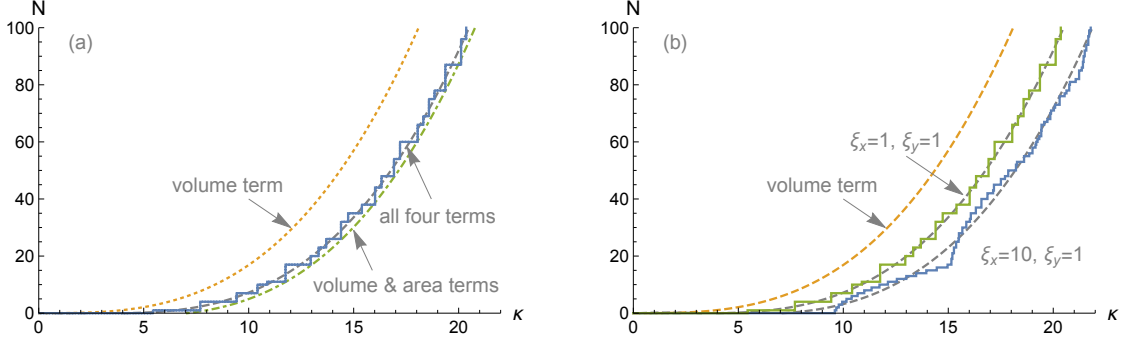


FIG. 2.  $N$  versus  $\kappa = kV^{1/3}$  for two rectangular domains. (a)  $(\xi_x, \xi_y) = (1, 1)$ , where  $\xi_{x,y} = L_{x,y}/L_z$ . The (blue) solid line shows the numerical data, which increases in discrete steps as new states are added. Also shown are various approximations from Eq. (19): the volume term (proportional to  $\kappa^3$ ), the volume and area terms, and all four terms. (b) Comparison of  $(\xi_x, \xi_y) = (1, 1)$  (a cube) and  $(\xi_x, \xi_y) = (10, 1)$  (a quasi-one-dimensional box). The dashed lines show the theoretical approximation from Eq. (19).

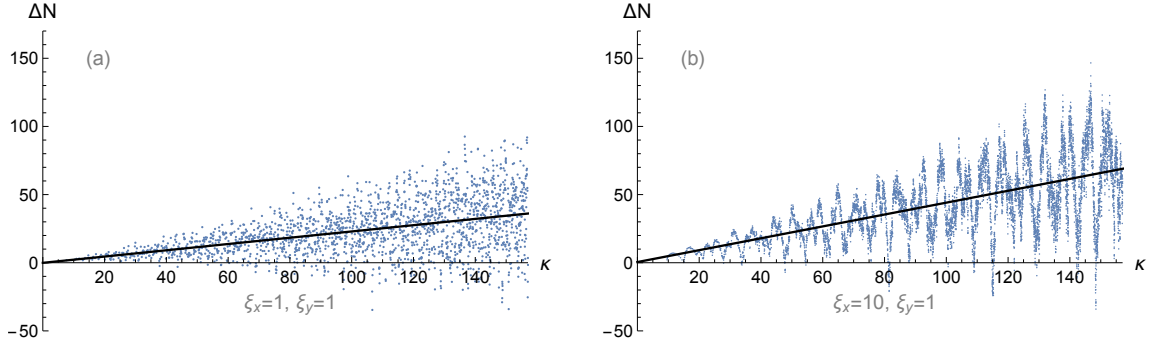


FIG. 3.  $\Delta N_{\text{rect}}$  defined in Eq. (22) versus  $\kappa$  for rectangular domains with (a)  $(\xi_x, \xi_y) = (1, 1)$  and (b)  $(\xi_x, \xi_y) = (10, 1)$ . The slopes of the best-fit lines give the coefficients of the linear terms in Eq. (19). The plot in (b) has far more points than that in (a) because the case  $(\xi_x, \xi_y) = (1, 1)$  has many degeneracies.

the Casimir effect, in which a sum over energy states can be written in terms of a mixture of continuous and discrete variables.<sup>17</sup> Further analysis of quasi-one- and two-dimensional systems is left for Problems 1.2, 1.3, 3.2 and 3.3.

To see the fluctuations about the asymptotic expression more clearly, we subtract the asymptotic expression from our exact (discrete) result for  $N(k)$ . If we define

$$\Delta N_{\text{rect}}(\kappa) \equiv N_{\text{rect}}(\kappa) - \frac{\kappa^3}{6\pi^2} + \kappa^2 f_{\text{rect}}^{(2)}(\xi_x, \xi_y), \quad (22)$$

	$f_{\text{rect}}^{(1)}(\xi_x, \xi_y)$	Linear Fit
$(\xi_x, \xi_y) = (1, 1)$	0.239	0.230
$(\xi_x, \xi_y) = (10, 1)$	0.443	0.436

TABLE II. Comparison of theoretical and fitted values for the coefficient of the linear term in Eq. (19) for the rectangular parallelepiped. The second column gives the slopes of the solid lines in Fig. 3. The fits include small constant terms as well, but these constants do not agree well with the expected value of  $-1/8$ .

the result should be approximately linear in  $\kappa$ ,

$$\Delta N_{\text{rect}}(\kappa) \sim \kappa f_{\text{rect}}^{(1)}(\xi_x, \xi_y) - \frac{1}{8}, \quad (23)$$

and we can perform a fit to determine the linear coefficient,  $f_{\text{rect}}^{(1)}(\xi_x, \xi_y)$  using our numerical data. Figure 3 shows plots of  $\Delta N_{\text{rect}}$ ; the results exhibit large fluctuations, as expected. Although the spread of  $\Delta N_{\text{rect}}$  values looks large on the scale used in Fig. 3, note that the vertical scale for  $N_{\text{rect}}$  would have a maximum of order  $6 \times 10^4$  for the same range of  $\kappa$  values.

The asymptotic expression in Eq. (19) implicitly assumes that an averaging procedure has been performed (see Ref. 22, for example). Rather than implement an involved averaging procedure, we adopt a simple-minded approach and simply fit a line to the points in the plots. Table II compares the slopes in Fig. 3 to the theoretical values. The agreement is good. To obtain good agreement, we had to implement a slightly improved prescription for  $N$ ,<sup>1</sup>

$$N(k) = \sum_{k_{\vec{n}} < k} 1 + \sum_{k_{\vec{n}} = k} \frac{1}{2} \quad (24)$$

[compare with Eq. (4)]. This revised prescription is particularly important for  $(\xi_x, \xi_y) = (1, 1)$ , which has large degeneracies. Using the original prescription in this case yields a linear coefficient that is more than 50% higher than the theoretical one.

## B. Sphere

For a sphere of radius  $a$  with Dirichlet boundary conditions, the wavenumbers are given by

$$k_{n\ell m}^2 = \frac{\beta_{\ell, n}^2}{a^2}, \quad (25)$$

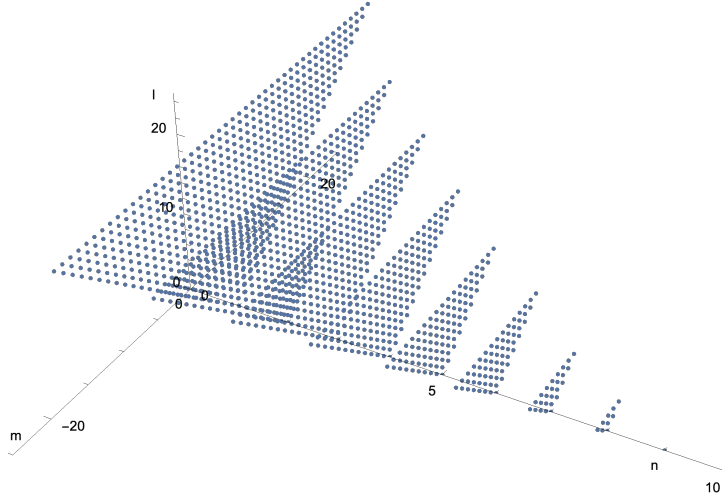


FIG. 4. States contributing to  $N(k)$  for a spherical volume with  $kV^{1/3} = 15\pi$ .  $N(k)$  is the sum of the 1561 points shown in the plot. The scales are different for the different directions, which gives the impression that the points are not uniformly spaced (which they are).

where  $\beta_{\ell,n}$  denotes the  $n$ th zero of the spherical Bessel function,  $j_\ell$ ; that is,  $j_\ell(\beta_{\ell,n}) = 0$  (see Appendix A 2). The integer  $\ell$  is related to the orbital angular momentum of the state and  $m$  is related to its azimuthal component. The quantum numbers take on the values  $n = 1, 2, 3, \dots$ ,  $\ell = 0, 1, 2, 3, \dots$  and  $m = -\ell, -\ell + 1, \dots, \ell - 1, \ell$ . The cumulative state number  $N(k)$  counts all of the states for which

$$\frac{\beta_{\ell,n}^2}{a^2} \leq k^2. \quad (26)$$

As is evident from Eq. (25), the quantized wavenumbers have a  $(2\ell + 1)$ -fold degeneracy, because the right-hand side does not depend on  $m$ . Thus, in actual computations of  $N(k)$ , we need only loop over  $\ell$  and  $n$  (being careful to keep track of the degeneracy).

It is useful to visualize the quantum numbers  $n$ ,  $\ell$  and  $m$  in terms of a three-dimensional lattice, as we did for the rectangular case. This approach is helpful for determining the volume and area terms in Eq. (8) (see Appendix C 1) and for visualizing the algorithm used to compute the cumulative state number. Figure 4 shows the states contributing to  $N(k)$  for  $kV^{1/3} = 15\pi$  (which is the same value that was used for Fig. 1).

We define the dimensionless variable  $\kappa$  as in Eq. (15) and express the eigenvalues as

$$\kappa_{n\ell m}^2 = \left(\frac{4\pi}{3}\right)^{2/3} \beta_{\ell,n}^2. \quad (27)$$

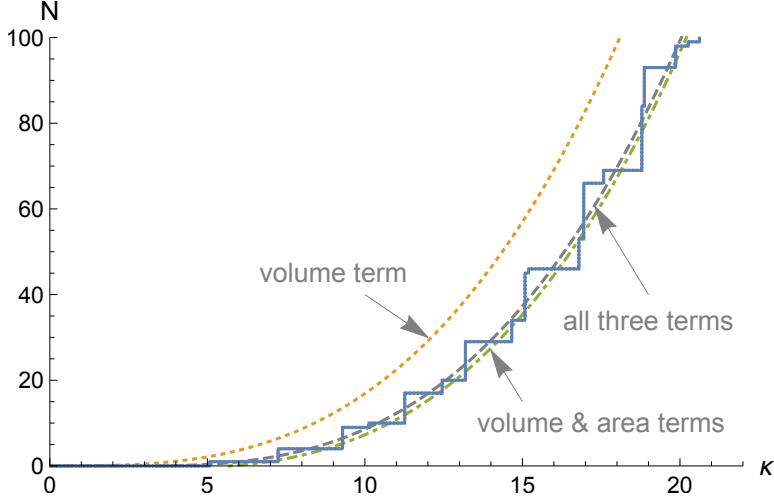


FIG. 5.  $N(\kappa)$  for a sphere. The smooth dashed lines show the theoretical result from Eq. (28), including one, two and three terms. Comparison with the analogous plots in Fig. 2 shows that the discrete steps are typically much larger in the present case due to the high degree of symmetry and the resulting  $(2\ell + 1)$ -fold degeneracies, which become large for large  $\ell$ . This effect also leads to large fluctuations when we calculate  $\Delta N_{\text{sph}}$ .

The asymptotic expression for the averaged cumulative state number becomes (see Table I)

$$\overline{N}_{\text{sph}}(\kappa) \sim \frac{\kappa^3}{6\pi^2} - \left(\frac{3}{32\pi}\right)^{2/3} \kappa^2 + \left(\frac{2}{9\pi^4}\right)^{1/3} \kappa + 0 + \dots \quad (28)$$

Figure 5 shows a plot of  $N(\kappa)$  as a function of  $\kappa$  for a sphere, with smooth curves showing the inclusion of various terms from Eq. (28). The plot looks similar to Fig. 5.2 in Ref. 15, which was considered in the context of a discussion on nuclear models. We can also define  $\Delta N_{\text{sph}}$  in analogy with Eq. (22) and use the result to determine the linear coefficient. This analysis is the subject of Projects 2.2 and 2.3. The fluctuations are very large in this case, due to the high degree of symmetry and the resulting large degeneracies in the eigenvalues.<sup>1</sup>

### C. Circular cylinder

The wavenumbers for a circular cylinder of radius  $a$  and length  $L$  with Dirichlet boundary conditions are given by

$$k_{nmn_z}^2 = \left(\frac{\zeta_{m,n}}{a}\right)^2 + \left(\frac{\pi n_z}{L}\right)^2, \quad (29)$$

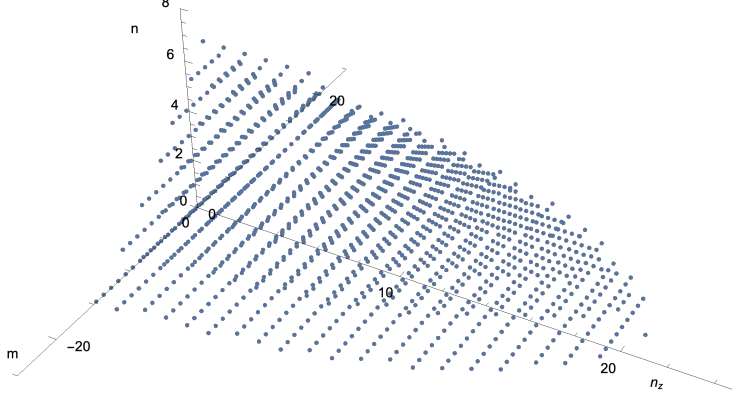


FIG. 6. The 1529 states contributing to  $N(k)$  for a cylindrical volume with  $kV^{1/3} = 15\pi$  and  $a = L/3$ . Note that  $n$  and  $n_z$  both start at one, while  $m$  includes positive and negative integers, as well as zero.

where  $\zeta_{m,n}$  denotes the  $n$ th zero of the regular Bessel function  $J_m$ ; that is,  $J_m(\zeta_{m,n}) = 0$  (see Appendix A 3). Also,  $n = 1, 2, 3, \dots$ ,  $n_z = 1, 2, 3, \dots$ , and  $m = 0, \pm 1, \pm 2, \dots$ . Figure 6 illustrates the states contributing to  $N(k)$  for  $kV^{1/3} = 15\pi$ , with  $a = L/3$ . The points corresponding to these states are uniformly spaced in  $n_z$ - $m$ - $n$  space and represent all of the states for which  $k_{nmn_z}^2 \leq (15\pi)^2/V^{2/3}$ . If we compare the values of  $N(k)$  for the parallelepiped, sphere and circular cylinder for the same value of  $kV^{1/3}$  (see Figs. 1, 4 and 6), we see that  $N(k) \approx 1500$  in each case, in accordance with Weyl's theorem.

We define  $\kappa$  as in Eq. (15) and express the eigenvalues as

$$\kappa_{nmn_z}^2 = \left(\frac{\pi}{\xi_a}\right)^{2/3} \zeta_{m,n}^2 + (\pi^4 \xi_a^2)^{2/3} n_z^2, \quad (30)$$

where we have defined  $\xi_a$  as

$$\xi_a = \frac{a}{L}. \quad (31)$$

The asymptotic expression for the averaged cumulative state number becomes

$$\overline{N}_{\text{cyl}}(\kappa) \sim \frac{\kappa^3}{6\pi^2} - \kappa^2 f_{\text{cyl}}^{(2)}(\xi_a) + \kappa f_{\text{cyl}}^{(1)}(\xi_a) + \frac{1}{256} \left( \frac{1}{\xi_a} - \frac{64}{3} \right) + \dots, \quad (32)$$

where

$$f_{\text{cyl}}^{(1)}(\xi_a) = \frac{1}{4\pi} \left[ \frac{2}{3} \left( \frac{1}{\pi \xi_a^2} \right)^{1/3} + (\pi^2 \xi_a)^{1/3} \right] \quad (33)$$

$$f_{\text{cyl}}^{(2)}(\xi_a) = \frac{1}{8\pi} \left[ (\pi \xi_a^2)^{1/3} + \left( \frac{\pi}{\xi_a} \right)^{1/3} \right]. \quad (34)$$

### III. PROJECTS AND PROBLEMS

In this section we outline several projects and problems. The projects are primarily computational in nature, and the problems focus on derivations and theoretical analyses of numerical results. The projects can be done without the problems, but the reverse is not true.

The projects and problems are more or less self-contained, although we recommend that Project 1.1 be done first. The code from this project can then be modified for the spherical and cylindrical cases, which have the complication that students need to determine the zeros of Bessel functions. For each geometry there is a project that focuses on determining the linear coefficient in the asymptotic expression for  $\overline{N}(\kappa)$ . This determination is challenging for the sphere, because the amplitude of the fluctuations is large in this case. Measurement of the linear coefficient for the spherical case spans Projects 2.2 and 2.3. In the first, students implement a much more efficient algorithm for determining  $N(\kappa)$ . In the second, they average  $\Delta N$  over small intervals and perform a weighted linear fit to the results.

In the following “calculate  $N(\kappa)$  as a function of  $\kappa$ ” means to determine a discrete set of ordered pairs  $(\kappa, N(\kappa))$  for the eigenvalues  $\kappa$ . This determination is not to be confused with calculating the corresponding averaged, asymptotic expression,  $\overline{N}(\kappa)$ , which is a continuous function of  $\kappa$ .

#### A. Rectangular parallelepiped

##### Problem 1.1 – Theoretical expressions

(a) Start from Eq. (9) and use the definitions of the dimensionless variables in Eqs. (15)–(17) to derive Eqs. (18) and (19).

(b) Determine the values of  $\xi_x$  and  $\xi_y$  that minimize  $f_{\text{rect}}^{(1)}(\xi_x, \xi_y)$  and  $f_{\text{rect}}^{(2)}(\xi_x, \xi_y)$ . What



shape is the bounding domain in this case?

### Project 1.1 – $N(\kappa)$ for a cube

Use the approach outlined in Appendix B1 and Algorithm 1 to find the 3719 states  $(n_x, n_y, n_z)$  that have  $\kappa_{n_x n_y n_z} \leq 20\pi$  for  $\xi_x = \xi_y = 1$  (set  $\kappa_{\max} = 20\pi$  in the algorithm). Generate plots similar to Figs. 1 and 2, including smooth curves corresponding to the inclusion of various terms from the asymptotic expression for  $\bar{N}_{\text{rect}}(\kappa)$  [see Eq. (19)]. As a first step, check that setting  $\kappa_{\max} = 4\pi$  yields the same 17 states described in Appendix B1. If you use *Mathematica*, a plot similar to Fig. 1 can be generated using `ListPointPlot3D[...]`.

### Project 1.2 – Quasi-one-dimensional geometry

Use your code from Project 1.1 to find  $N(\kappa)$  as a function of  $\kappa$  for  $\xi_x = 50$  and  $\xi_y = 1$ , setting  $\kappa_{\max} = 12\pi$ . In this case the  $x$  dimension of the box is fifty times larger than the  $y$  and  $z$  dimensions, so the box is quasi-one-dimensional. Plot  $N(\kappa)$  as in Fig. 2. You should see prominent cusps near  $\kappa \approx 26$  and  $\kappa \approx 33$ .

### Problem 1.2 – Analysis of a quasi-one-dimensional geometry

(a) Use Eq. (18) to derive an expression for  $N(\kappa)$  in the region between  $\kappa \approx 16$  and the cusp at  $\kappa \approx 26$  in Project 1.2. Hint: In this region,  $n_y = n_z = 1$ , so  $N = n_x$ . Superimpose your theoretical expression on the plot of the data obtained in Project 1.2.

(b) Use Eq. (18) to calculate  $\kappa$  and  $N$  for the cusp near  $\kappa \approx 26$ . The cusp occurs when  $n_y$  and  $n_z$  begin to take on values other than 1. (The idea is to calculate the location of the cusp, which will be close to  $\kappa = 26$ .)

(c) (More difficult) Use Eq. (18) to determine  $N(\kappa)$  as a function of  $\kappa$  between the cusps near  $\kappa \approx 26$  and  $\kappa \approx 33$ . Superimpose your result on the plot of the data obtained in Project 1.2.

(d) Use Eq. (18) to calculate  $\kappa$  for the cusp near  $\kappa \approx 33$ . What is the reason for the cusp in this case?

### Project 1.3 – Linear coefficient for the quasi-one-dimensional geometry

Calculate  $N(\kappa)$  for  $\xi_x = 50$  and  $\xi_y = 1$  (as in Project 1.2) to at least  $\kappa_{\max} = 40\pi$ . Subtract the volume and area terms from  $N(\kappa)$  to obtain  $\Delta N$  [see Eq. (22)]. Plot  $\Delta N$  as a function of  $\kappa$  and do a linear fit. Compare your result to the expression for the linear coefficient in Eq. (20) [that is, compare your slope to  $f_{\text{rect}}^{(1)}(50, 1)$ ]. The two results should agree to within

5%. In principle you should use the improved prescription for determining  $N(\kappa)$  here (see the discussion at the end of Appendix B 1), although it does not make much difference in this case.

### **Project 1.4 – Quasi-two-dimensional geometry**

This project can be done immediately after Project 1.1, although it would be helpful to have read Project 1.2 first. Use your code from Project 1.1 to find  $N(\kappa)$  as a function of  $\kappa$  for  $\xi_x = 1/50$  and  $\xi_y = 1$ , setting  $\kappa_{\max} = 30\pi$ . In this case the  $x$  dimension is one fiftieth the length of the  $y$  and  $z$  dimensions, so the box is quasi-two-dimensional. Plot  $N(\kappa)$  as a function of  $\kappa$  and superimpose the theoretical asymptotic expression. You should see a cusp near  $\kappa \approx 85$ .

### **Problem 1.3 – Analysis of the quasi-two-dimensional case (difficult)**

(a) Calculate the approximate location of the cusp near  $\kappa \approx 85$ , and determine  $N(\kappa)$  for  $\kappa$  between  $\kappa \approx 43$  and  $\kappa \approx 85$ . You will probably need to do a continuum approximation for  $n_y$  and  $n_z$ . Superimpose your plot on the exact result obtained in Project 1.4.

(b) Determine an approximate expression for  $N(\kappa)$  for  $\kappa$  between  $\kappa \approx 85$  and the next cusp. Superimpose your result on the exact result.

(c) Generalize your result to find an approximate expression for  $N(\kappa)$  between any two cusps. Use your result to recover the volume term in Eq. (19), showing that this quasi-two-dimensional example approaches the usual result for large  $\kappa$ .

## **B. Sphere**

### **Problem 2.1 – Theoretical expressions**

Start from Eqs. (15) and (25) and derive Eqs. (27) and (28).

### **Project 2.1 – $N(\kappa)$**

Modify your code from Project 1.1 and follow the approach in Appendix B 2 to find the 3818 states  $(n, m, \ell)$  that have  $\kappa_{nlm} \leq 20\pi$  for the spherical case. Generate plots similar to Figs. 4 and 5, including smooth curves corresponding to the inclusion of various terms from the asymptotic expression for  $\overline{N}_{\text{sph}}(\kappa)$ , Eq. (28).

### **Project 2.2 – An efficient algorithm**

Implement a much more efficient algorithm for the spherical case.

(a) Use the algorithm outlined in Appendix B 3 a to determine the number of states with  $\kappa_{n\ell m} \leq 20\pi$ . Your answer should agree with what you found in Project 2.1. Also, determine the largest eigenvalue  $\kappa_{n\ell m}$  that is less than or equal to  $20\pi$ . You will probably find that your algorithm runs much more quickly than your previous one.

(b) Repeat for  $\kappa_{\max} = 500$ . Calculate the percentage difference between your value for  $N$  and the theoretical expression in Eq. (28). (Run your code from Project 2.1 for  $\kappa_{\max} = 500$  so that you can compare the run times.)

### Project 2.3 – Numerical determination of the linear coefficient (difficult)

The goal of this project, which extends Project 2.2, is to determine the linear coefficient in Eq. (28) numerically. A complicating factor in the spherical case is that it is necessary to go to large values of  $\kappa$  to obtain a reasonable result. Rather than calculating  $\Delta N$  for all values of  $\kappa$  over some large range and performing a linear fit (as in Fig. 3), calculate  $\Delta N$  over a sequence of small intervals (for example,  $\kappa \in (20, 30), (120, 130), \dots$ ) Then consolidate the data in those ranges by computing averages, and do a linear fit to those points.

(a) Implement the algorithm described in Appendix B 3 b for  $\kappa_{\min} = 100$  and  $\kappa_{\max} = 120$ . Average the values as described there to determine  $\bar{\kappa}$  and  $\overline{\Delta N}$  (along with its uncertainty). Embed your algorithm in a function so that it can be called for any value of  $\kappa_{\min}$  and  $\kappa_{\max}$ .

(b) Determine  $\bar{\kappa}$  and  $\overline{\Delta N}$  (along with its uncertainty) for  $\kappa \in (20, 30), \kappa \in (120, 130), \dots, \kappa \in (420, 430), \dots$ . Plot your  $(\bar{\kappa}, \overline{\Delta N})$  pairs, including error bars in the vertical direction. The data should look reasonably linear if the error bars are taken into account.

(c) Do a weighted linear fit to your data from part (b) taking into account the uncertainties of the  $\overline{\Delta N}$  values.<sup>27</sup> Superimpose the fit on your plot from part (b). Compare the slope that you obtain to the linear coefficient in Eq. (28).

## C. Cylinder

### Problem 3.1 – Theoretical expressions

(a) Start from Eq. (29) and the definitions in Eqs. (15) and (31) and derive Eqs. (30) and (32).

(b) Determine the value of  $\xi_a$  that minimizes  $f_{\text{cyl}}^{(2)}(\xi_a)$ . (This value of  $\xi_a$  minimizes the surface area of the cylinder for a given volume.)

### Project 3.1 – $N(\kappa)$

Modify your code from Project 1.1 and follow the approach in Appendix B 2 to find the 3761 states  $(n_z, m, n)$  that have  $\kappa_{nmn_z} \leq 20\pi$  for the cylindrical case, with  $\xi_a = 1/3$ . Generate plots similar to Figs. 5 and 6, including smooth curves corresponding to the inclusion of various terms from the asymptotic expression for  $\overline{N}_{\text{cyl}}(\kappa)$ , Eq. (32).

### Project 3.2 – Linear coefficient (difficult)

Calculate  $N(\kappa)$  for  $\xi_a = 1/3$  (as in Project 3.1). Reasonable results for the linear coefficient can be obtained by choosing  $\kappa_{\text{max}} = 20\pi$ ; better agreement will be obtained by choosing  $\kappa_{\text{max}} = 150$ , but the computation time will be long. Subtract the volume and area terms in Eq. (32) from  $N(\kappa)$  to obtain  $\Delta N$ . Plot  $\Delta N$  as a function of  $\kappa$  and do a linear fit to this data. Compare your result to the expression for the linear coefficient in Eq. (33) [that is, compare your slope to  $f_{\text{cyl}}^{(1)}(1/3)$ ]. In principle, you should use the improved prescription for determining  $N(\kappa)$  here (see the discussion at the end of Appendix B 1), although in practice it does not make much difference in this case.

### Project 3.3 – A quantum wire

Use your code from Project 3.1 to find  $N(\kappa)$  for  $\xi_a = 1/200$  with  $\kappa_{\text{max}} = 50$ . The length of the cylinder is 200 times larger than its radius, so the cylinder is quasi-one-dimensional. Plot  $N(\kappa)$  and superimpose smooth curves corresponding to the inclusion of various terms from the asymptotic expression, Eq. (32). You should see prominent cusps near  $\kappa \approx 33$  and  $\kappa \approx 44$ .

### Problem 3.2 – Analysis of a quantum wire

This problem is related to Project 3.3. Analytically determine the locations of the cusps near  $\kappa \approx 33$  and  $\kappa \approx 44$ . (See Problem 1.2 for help getting started.)

### Project 3.4 – A thin disk

Use your code from Project 3.1 to find  $N(\kappa)$  for  $\xi_a = 15$ , setting  $\kappa_{\text{max}} = 60$ . The length of the cylinder is 15 times smaller than its radius, so the cylinder is quasi-two-dimensional. You should see a cusp near  $\kappa \approx 56$ .

### Problem 3.3 – Analysis of a thin disk (very difficult)

This problem is related to Project 3.4. Analytically determine the location of the cusp near  $\kappa \approx 56$  and obtain an analytical expression for  $N(\kappa)$  for  $\kappa$  between  $\kappa \approx 28$  and  $\kappa \approx 56$ . (To calculate  $N(\kappa)$  you will need to follow an approach similar to that in Appendix C 2.)

#### IV. DISCUSSION AND CONCLUDING REMARKS

In this work we presented algorithms to compute the cumulative state number,  $N(k)$ , for a rectangular box, a sphere and a cylinder. In each case  $N(k)$  is discrete and may be computed by summing a set of points on a lattice in three dimensions. Through projects and problems described here, students can calculate  $N(k)$  and compare their exact results with various terms in the asymptotic expression. As noted in Sec. I  $N(k)$  and its derivative, the density of states, have many applications in a wide range of physical contexts. Our analysis has been in the context of non-relativistic quantum mechanics, but there are also classical applications (in acoustics) and important relativistic applications, including blackbody radiation and the Casimir effect.<sup>1,3,16</sup>

We emphasized the analysis of quasi-one- and two-dimensional bounding domains, for which  $N(k)$  shows a mixture of discrete and continuum-like behavior due to quantum numbers associated with the small and large dimensions, respectively. Plots of  $N(k)$  contain cusps that indicate changes in the quantum numbers associated with the small dimensions. Students can derive analytical expressions that describe the regions between the cusps; in the quasi-two-dimensional cases, the large  $k$  behavior of these expressions reduces to the leading term in the asymptotic expression, verifying Weyl's theorem. Nanostructures can be fabricated that approximate one- and two-dimensional systems. Reference 28 contains an experimental study and analysis of the quasi-one-dimensional density of states in a quantum ring. Although the situation there is much more complicated than those considered here, we note an interesting discussion in that paper regarding the effect of the finite rim width compared to the ring circumference.

There are several ways in which the projects in this work can be extended or generalized. Here we list a few possibilities.

1. **Two dimensions.** The asymptotic expression for the average cumulative state number is well known in two dimensions, so we can consider, for example, rectangular and

circular domains and analyze the agreement between the exact and asymptotic results. See Ref. 1, pp. 59–63 as a starting point.

2. **Electromagnetic problem.** We have implicitly considered what is called the scalar version of the problem, but we can also consider the electromagnetic version of the problem, which is important for blackbody radiation. In this case we need to consider correlated electric and magnetic fields, and their corresponding boundary conditions. See Ref. 1 and references therein.
3. **Bubble/thick-shell example.** The theoretical discussion in Ref. 10 can be used to solve for the eigenvalues of wave functions inside a spherical shell with Dirichlet boundary conditions. Reference 1 and references therein contain useful information for determining the asymptotic expression for the averaged cumulative state number. Reference 8 could also be helpful (but the results in Ref. 8 are written in terms of a time variable; see Ref. 1, pp. 30–31.)
4. **A complementary method of determining  $N$  in the spherical case.** We can use Eq. (C.3) with the factor of  $1/4$  replaced by  $\chi/\pi$  to determine  $n$  versus  $\ell$  (for integer  $\ell$  values) for the spherical case. Rounding the  $n$  values down to integers gives an accurate boundary that can then be used to determine the exact number of states without determining the zeros of Bessel functions (which is computationally expensive). The trick is that  $\chi$  must be determined accurately, which can be done by computing a line integral in the complex plane, as described in Ref. 29.

## ACKNOWLEDGMENTS

KK thanks Taylor University for its support during his sabbatical. The authors thank Daniel Schroeder for helpful feedback. Solutions to the problems and sample code for the projects are available upon request by sending an email to KK.

## Appendix A: Summary of Energy Eigenfunctions

We list the energy eigenfunctions and eigenvalues (the solutions to Eq. (2) with Dirichlet boundary conditions) for the three geometries considered in this work. The rectangular case

is a straightforward generalization of the one-dimensional version. Results for the spherical and cylindrical cases may be found, for example, in Refs. 12 and 30.

### 1. Rectangular parallelepiped

The energy eigenfunctions in the rectangular domain  $0 \leq x \leq L_x$ ,  $0 \leq y \leq L_y$  and  $0 \leq z \leq L_z$  are given by

$$\psi_{n_x n_y n_z}(x, y, z) = A_{n_x n_y n_z} \sin\left(\frac{n_x \pi x}{L_x}\right) \sin\left(\frac{n_y \pi y}{L_y}\right) \sin\left(\frac{n_z \pi z}{L_z}\right), \quad (\text{A.1})$$

where  $A_{n_x n_y n_z}$  is a normalization constant and the integers  $n_x$ ,  $n_y$  and  $n_z$  can independently take on the values  $1, 2, 3, \dots$ . The corresponding energy eigenvalues are given by

$$\epsilon_{n_x n_y n_z} = \frac{\hbar^2 \pi^2}{2\mu} \left( \frac{n_x^2}{L_x^2} + \frac{n_y^2}{L_y^2} + \frac{n_z^2}{L_z^2} \right). \quad (\text{A.2})$$

### 2. Sphere

The energy eigenfunctions inside the spherical domain  $r \leq a$  are given by

$$\psi_{n\ell m}(r, \theta, \phi) = A_{n\ell m} Y_{\ell m}(\theta, \phi) j_\ell(\beta_{\ell, n} r/a), \quad (\text{A.3})$$

where  $A_{n\ell m}$  is a normalization constant,  $Y_{\ell m}(\theta, \phi)$  is a spherical harmonic and  $j_\ell(\beta_{\ell, n} r/a)$  is the spherical Bessel function of order  $\ell$ .  $\beta_{\ell, n}$  is the  $n$ th zero of  $j_\ell$ . The quantum numbers are given by  $n = 1, 2, 3, \dots$ ,  $\ell = 0, 1, 2, \dots$  and  $m = -\ell, -\ell + 1, \dots, \ell$ . The energy eigenvalue corresponding to the state  $\psi_{n\ell m}$  is  $\epsilon_{n\ell m} = \hbar^2 \beta_{\ell, n}^2 / (2\mu a^2)$ . The energy eigenstates are  $(2\ell + 1)$ -fold degenerate, because the corresponding energy eigenvalues do not depend on  $m$ .

### 3. Circular cylinder

The energy eigenfunctions inside the cylindrical domain bounded by  $r \leq a$  and  $0 \leq z \leq L$  are given in cylindrical coordinates by

$$\psi_{nmn_z}(r, \phi, z) = A_{nmn_z} J_m(\zeta_{m, n} r/a) e^{im\phi} \sin\left(\frac{n_z \pi z}{L}\right), \quad (\text{A.4})$$

where  $A_{nmn_z}$  is a normalization constant,  $J_m(\zeta_{m,n}r/a)$  is the Bessel function of order  $m$ , and  $\zeta_{m,n}$  is the  $n$ th zero of  $J_m$ . The quantum numbers can take on the integer values  $n = 1, 2, 3, \dots$ ,  $m = 0, \pm 1, \pm 2, \dots$  and  $n_z = 1, 2, 3, \dots$  and the energy eigenvalues are

$$\epsilon_{nmn_z} = \frac{\hbar^2}{2\mu} \left( \frac{\zeta_{m,n}^2}{a^2} + \frac{\pi^2 n_z^2}{L^2} \right). \quad (\text{A.5})$$

Note that  $J_{-m}(x) = (-1)^m J_m(x)$  for  $m = 1, 2, 3, \dots$ ,<sup>33</sup> meaning that  $J_{-m}$  and  $J_m$  have zeros at the same locations. Thus, the energy eigenvalues have a two-fold degeneracy for each  $m \neq 0$ .

## Appendix B: Pseudocode for determining $N$

### 1. The rectangular case

$N(\kappa)$  is the number of states with  $\kappa_{n_x n_y n_z}^2 \leq \kappa^2$  [see the definition of  $\kappa_{n_x n_y n_z}^2$  in Eq. (18)]. Our goal is to find  $N(\kappa_{\max})$  and  $N(\kappa)$  for all  $\kappa \leq \kappa_{\max}$ . We need to be careful not to miss contributing states. In Algorithm 1 we use several embedded **While** loops and are careful to set appropriate exit conditions so that the program does not become stuck in an infinite loop.<sup>31</sup> We can visualize the algorithm with the aid of Fig. 1. We start at the point  $(n_x, n_y, n_z) = (1, 1, 1)$  and increase  $n_z$  until we reach the maximum value allowed by  $\kappa_{\max}$ . We then move to  $(n_x, n_y, n_z) = (1, 2, 1)$  and do the same until the entire back “wall” (with  $n_x = 1$ ) has been filled in. At that point we increment  $n_x$  and continue in the same manner until all of the states have been found. We have implemented the algorithm in **Mathematica** and **Python**. In **Mathematica**, the sorting and splitting can be done in a single step using `Split[Sort[dataArray, #1<#2 &]]`.<sup>32</sup> We set  $\kappa_{\max} = 4\pi$  and  $\xi_x = \xi_y = 1$  and obtain the



following results for several of the arrays in the pseudocode,

$$\begin{array}{ccccc}
\begin{pmatrix} 1 & 1 & 1 \\ 1 & 1 & 2 \\ 1 & 1 & 3 \\ 1 & 2 & 1 \\ 1 & 2 & 2 \\ 1 & 2 & 3 \\ 1 & 3 & 1 \\ 1 & 3 & 2 \\ 2 & 1 & 1 \\ \vdots \end{pmatrix} & 
\begin{pmatrix} 3\pi^2 \\ 6\pi^2 \\ 11\pi^2 \\ 6\pi^2 \\ 9\pi^2 \\ 14\pi^2 \\ 11\pi^2 \\ 14\pi^2 \\ 6\pi^2 \\ \vdots \end{pmatrix} & 
\begin{pmatrix} 3\pi^2 \\ 6\pi^2 \\ 6\pi^2 \\ 6\pi^2 \\ 9\pi^2 \\ 9\pi^2 \\ 9\pi^2 \\ 11\pi^2 \\ 11\pi^2 \\ \vdots \end{pmatrix} & 
\begin{pmatrix} \{3\pi^2\} \\ \{6\pi^2, 6\pi^2, 6\pi^2\} \\ \{9\pi^2, 9\pi^2, 9\pi^2\} \\ \{11\pi^2, 11\pi^2, 11\pi^2\} \\ \{12\pi^2\} \\ \{14\pi^2, 14\pi^2, 14\pi^2, \\ 14\pi^2, 14\pi^2, 14\pi^2\} \end{pmatrix} & 
\begin{pmatrix} 5.4414 & 1 \\ 7.6953 & 4 \\ 9.42478 & 7 \\ 10.4195 & 10 \\ 10.8828 & 11 \\ 11.7548 & 17 \end{pmatrix}, \quad (B.1) \\
\text{array \#1} & \text{array \#2} & \text{array \#3} & \text{array \#4} & \text{array \#5}
\end{array}$$

where **array #1** contains the triplets  $(n_x, n_y, n_z)$  (which can be used to generate a plot such as Fig. 1), **array #2** (**#3**) contains the unsorted (sorted)  $\kappa_{n_x n_y n_z}^2$  values, **array #4** contains the “sorted and split” values of  $\kappa^2$  (note the degeneracies), and **array #5** contains  $(\kappa, N(\kappa))$  pairs (which can be used to generate a plot such as Fig. 2). Note that  $N(\kappa)$  is the number of states up to and including a particular value of  $\kappa$ .

To determine the coefficient of the linear term in Eq. (19), it is important to use the improved prescription for calculating  $N$  that is defined in Eq. (24), instead of the original one defined in Eq. (4). Algorithm 1 uses the unimproved prescription, but it is straightforward to fix this by averaging successive  $N$  values in the array containing the  $\kappa$  and  $N$  values. For example, for the above data set, averaging yields:

$$\begin{pmatrix} 5.4414 & 1 \\ 7.6953 & 4 \\ 9.42478 & 7 \\ 10.4195 & 10 \\ 10.8828 & 11 \\ 11.7548 & 17 \end{pmatrix} \rightarrow \begin{pmatrix} 5.4414 & 0.5 \\ 7.6953 & 2.5 \\ 9.42478 & 5.5 \\ 10.4195 & 8.5 \\ 10.8828 & 10.5 \\ 11.7548 & 14 \end{pmatrix}. \quad (B.2)$$

Subtracting the volume and area terms from the  $N(\kappa)$  values in the second array yields  $\Delta N$

[see Eq. (22)], which can then be used to produce a plot such as Fig. 3.

```

set kappaMax, xix and xiy;
initialize array #1 (stores (nx,ny,nz) satisfying kappaSq<=kappaMax^2);
initialize array #2 (stores kappaSq values);
nx=1;
nxOK=true;
while nxOK do:
| ny=1;
| nyOK=true;
| while nyOK do:
| | nz=1;
| | nzOK=true;
| | while nzOK do:
| | | kappaSq=pi^2(nx^2(xiy/xix^2)^(2/3)+...);
| | | if kappaSq>kappaMax^2 then:
| | | | nzOK=false;
| | | | if nz==1 then:
| | | | | nyOK=false;
| | | | | if ny==1 then:
| | | | | | nxOK=false;
| | | | | else:
| | | | | | increment nx;
| | | | | end;
| | | | else:
| | | | | increment ny;
| | | | end;
| | | else:
| | | | append (nx,ny,nz) to array #1;
| | | | append kappaSq to array #2;
| | | | increment nz;
| | | end;
| | end;
| end;
end;
sort array #2 by increasing values of kappaSq; store as array #3;
split array #3 into sets of degenerate values; store as array #4;
initialize array #5 (stores (kappa,N) pairs);
loop through array #4; count states and append results to array #5;

```

**Algorithm 1:** An algorithm to find all states in a rectangular parallelepiped that have  $\kappa_{n_x n_y n_z}$  less than or equal to  $\kappa_{\max}$ . The states are sorted by increasing  $\kappa$  and then degenerate states are collected into groups. Array #1 [which stores  $(n_x, n_y, n_z)$  values] can be used to generate a figure such as Fig. 1, but is otherwise not needed. Array #5 [which contains  $(\kappa, N(\kappa))$  pairs] can be used to generate figures such as Fig. 2.

## 2. Algorithms for the spherical and cylindrical geometries

The approach in Algorithm 1 can be adapted for the spherical and cylindrical cases with some small changes. For the spherical case, we replace  $\kappa_{n_x n_y n_z}$  by  $\kappa_{n\ell m}$ , and in the **While** loops, we replace  $n_x$  by  $n$  and  $n_y$  by  $\ell$  [see Eq. (27) and Fig. 4]. The inner **While** loop in Algorithm 1 is not necessary and can be replaced by a **Do** loop for  $m$  ranging from  $-\ell$  to  $\ell$ . (If only states are counted, in contrast to generating a plot such as Fig. 4, we can include a degeneracy factor.) Another small change is that  $\ell$  starts at 0 ( $n_y$  starts at 1). **Mathematica** has a function that returns the  $n$ th zero of the regular Bessel function. Because  $j_\ell(x) \propto x^{-1/2} J_{\ell+1/2}(x)$ ,<sup>33</sup> finding the  $n$ th zero of  $j_\ell$  is equivalent to finding the  $n$ th zero of  $J_{\ell+1/2}$ . In **Mathematica**  $\beta_{\ell,n} = \text{BesselJZero}[\ell + 1/2, n]$ . For a useful algorithm in **Python** see the **SciPy Cookbook**.<sup>34</sup>

For the cylindrical case, we replace  $\kappa_{n_x n_y n_z}$  by  $\kappa_{nmn_z}$ , and in the **While** loops, we replace  $n_x$  by  $n_z$ ,  $n_y$  by  $m$ , and  $n_z$  by  $n$ , noting that  $n_z$  starts at 1,  $m$  is symmetrically distributed about 0 and  $n$  starts at 1 [see Eq. (30) and Fig. 6]. For  $m$ , we can start at zero and increment through positive values, remembering to include an extra state  $-m$  for every state  $m$  when  $m > 0$ .

## 3. More efficient algorithms for spherical geometry

The straightforward, brute force algorithms we have described become computationally expensive for large  $\kappa$ . Furthermore, for the spherical case, the difference between  $N(\kappa)$  and the averaged approximation in Eq. (28) is highly oscillatory. If we wish to perform a fit to determine the linear coefficient numerically for the spherical case, we need to go to large values of  $\kappa$ . Fortunately, we can employ a much more efficient algorithm if we are interested only in determining  $N$  for a particular value of  $\kappa$  or for a small range of  $\kappa$  values.

### *a. $N$ for one value of $\kappa$*

The pseudocode in Algorithm 2 efficiently determines  $N$  for a given value  $\kappa_{\text{max}}$ . This algorithm is based on three observations, the first two of which may be understood by examining Fig. 4:

1. For a given value of  $\kappa_{\max}$ , the maximum value of  $\ell$  is a monotonically decreasing function of  $n$ . (In Fig. 4, the triangles become smaller as  $n$  gets larger.)
2. Once the maximum value of  $\ell$  is known for a given value of  $n$ , the number of points in the corresponding triangle in  $(n, m, \ell)$ -space can be calculated immediately and is given by

$$\sum_{\ell=0}^{\ell_{\max}} (2\ell + 1) = (\ell_{\max} + 1)^2, \quad (\text{B.3})$$

where  $\ell_{\max}$  is the maximum value of  $\ell$  for a given value of  $n$ .

3. The zeros of the spherical Bessel functions,  $\beta_{\ell,n}$ , satisfy the inequality  $\beta_{\ell,n} \geq \ell + \frac{1}{2}$ .<sup>29</sup> For  $n = 1$ ,  $\ell_{\max}$  is less than  $(3/(4\pi))^{1/3} \kappa_{\max}$  [see Eq. (27)].

The idea of the algorithm is to start at  $n = 1$  and set  $\ell$  equal to an integer slightly greater than  $(3/(4\pi))^{1/3} \kappa_{\max}$ . To determine  $\ell_{\max}$ , we decrease  $\ell$  in unit steps until  $\beta_{\ell,1}$  is less than or equal to  $(3/(4\pi))^{1/3} \kappa_{\max}$ . Having found  $\ell_{\max}$  for  $n = 1$ , we add up the number of states for this triangle [see Eq. (B.3)] and proceed to  $n = 2$ , decreasing  $\ell$  as necessary until  $\beta_{\ell,2}$  is less than or equal to  $(3/(4\pi))^{1/3} \kappa_{\max}$ .

```

set kappaMax;
initialize N to zero, n to 1, and kappaLargest to zero;
lMax=Ceiling((3/(4pi))^(1/3)kappaMax);
while lMax>-1 do:
|  solutionFound=false;
|  while ((not solutionFound) and (lMax>-1)) do:
|  |  betalMaxn=nth zero of spherical Bessel function;
|  |  kappa=(4pi/3)^(1/3)betalMaxn;
|  |  if kappa<=kappaMax then:
|  |  |  if kappa>kappaLargest then:
|  |  |  |  kappaLargest=kappa;
|  |  |  end;
|  |  |  increment N by (lMax+1)^2;
|  |  |  solutionFound=true;
|  |  else:
|  |  |  decrement lMax;
|  |  end;
|  end;
|  increment n;
end;

```

**Algorithm 2:** An efficient algorithm to determine  $N$ , the number of states in a sphere, for  $\kappa_{n\ell m} \leq \kappa_{\max}$ . The algorithm returns  $N$  and the largest value of  $\kappa_{n\ell m}$  encountered,  $\kappa_{\text{largest}}$ .

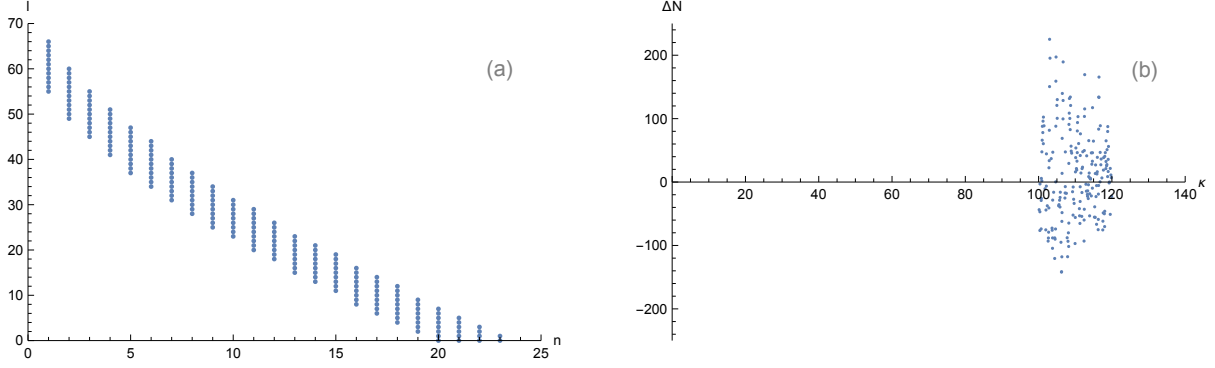


FIG. 7. (a) States with  $100 \leq \kappa_{nlm} \leq 120$  for a spherical volume. The  $m$  direction has been suppressed, meaning that each dot represents  $(2\ell + 1)$  states. (b)  $\Delta N$  as a function of  $\kappa$  for the states shown in (a). To obtain  $\Delta N$ , we have subtracted the volume ( $\sim \kappa^3$ ) and surface area ( $\sim \kappa^2$ ) terms shown in Eq. (28). For Project 2.3 we consolidate all of these points by averaging them, which yields  $(\bar{\kappa}, \overline{\Delta N}) \simeq (110.229, 11.6 \pm 4.9)$ .

*b.  $N$  for a range of  $\kappa$  values*

In Project 2.3 we must determine all  $(\kappa, N(\kappa))$  pairs for  $\kappa_{\min} \leq \kappa \leq \kappa_{\max}$ . Algorithm 2 can be adapted for this task with some small adjustments. Instead of immediately incrementing  $n$  once a solution has been found for some value of  $\ell$ , we continue to decrement  $\ell$  until  $\kappa < \kappa_{\min}$  (or  $\ell$  becomes negative). The values of  $n$ ,  $\ell$  and  $\kappa$  can be stored in an array, which can then be sorted in order of increasing  $\kappa$  values. Because  $N$  is known for the largest value of  $\kappa$ , the values of  $N$  for the other  $\kappa$  values can be determined by traversing the sorted array (backwards) and subtracting appropriate values of  $(2\ell + 1)$  from the running value of  $N$  at each step.

As an example, suppose we wish to find all of the  $(\kappa, N(\kappa))$  pairs with  $100 \leq \kappa \leq 120$ . Figure 7(a) shows the corresponding states in the  $(n, \ell)$  plane (each point represents  $(2\ell + 1)$  states, because we have suppressed the  $m$  direction in the plot). The largest value of  $\kappa$  in this range is  $\approx 119.933$ , and corresponds to  $(n, \ell) = (15, 19)$  and  $N = 27,745$ . The next largest value of  $\kappa$  is  $\approx 119.846$  and the corresponding value of  $N$  is thus  $27,745 - (2 \times 19 + 1) = 27,706$ .

Continuing in this way yields the  $(n, \ell, \kappa, N)$  array in the following:

$$\begin{array}{ccc}
\begin{pmatrix} 5 & 37 & 100.146 & 15,990 \\ 9 & 25 & 100.342 & 16,041 \\ \vdots & \vdots & \vdots & \vdots \\ 6 & 44 & 119.555 & 27,548 \\ 1 & 66 & 119.728 & 27,681 \\ 18 & 12 & 119.846 & 27,706 \\ 15 & 19 & 119.933 & 27,745 \end{pmatrix} & \rightarrow & \begin{pmatrix} 100.146 & 15,952.5 \\ 100.342 & 16,015.5 \\ \vdots & \vdots \\ 119.555 & 27,503.5 \\ 119.728 & 27,614.5 \\ 119.846 & 27,693.5 \\ 119.933 & 27,725.5 \end{pmatrix} & \rightarrow & \begin{pmatrix} 100.146 & -43.593 \\ 100.342 & -76.382 \\ \vdots & \vdots \\ 119.555 & 21.482 \\ 119.728 & 11.113 \\ 119.846 & 6.858 \\ 119.933 & -22.426 \end{pmatrix} \\
(n, \ell, \kappa, N) & & (\kappa, N_{\text{improved}}) & & (\kappa, \Delta N)
\end{array} \quad (\text{B.4})$$

For Project 2.3 we need to manipulate the data in the  $(n, \ell, \kappa, N)$  array to determine average values for  $\kappa$  and  $\Delta N$ . In the  $(\kappa, N_{\text{improved}})$  array we implement the improved definition of  $N$  [see Eq. (24) and also the discussion in Appendix B 1; note that in this case we can subtract appropriate values of  $(2\ell+1)/2$ ]. Then we subtract the volume and area terms in Eq. (28) to determine  $\Delta N$ . The result is shown in the  $(\kappa, \Delta N)$  array above and is plotted in Fig. 7(b). The  $\Delta N$  values are highly oscillatory. Finally, we determine the mean values of the  $(\kappa, \Delta N)$  array, which yields  $(\bar{\kappa}, \overline{\Delta N}) \simeq (110.229, 11.6 \pm 4.9)$ . To estimate the uncertainty in  $\overline{\Delta N}$ , we have computed the standard deviation and divided by the square root of 208 (which is the number of data points that are being averaged). Note that the amplitude of the oscillations in  $\Delta N$  is much greater than the mean value.

### Appendix C: The volume and surface area terms for the spherical and cylindrical cases

In this appendix we provide a quasi-rigorous derivation of the volume and surface area terms in Eq. (8) for a sphere and cylinder.<sup>35</sup> Reference 30 contains similar calculations for the density of states  $dN(k)/dk$ , but only of the volume term.<sup>36</sup> Because we calculate both the volume and the surface area terms, we need to be more careful how the bounding surfaces are treated. Also, Ref. 30 neglects the dependence on  $\chi$  [see Eq. (C.1)], but we find that this quantity must be treated carefully to obtain the correct expression for the surface area terms.

## 1. Sphere

It is nontrivial to determine the volume of the lattice points bounded by a particular choice of  $k$  in the large  $k$  limit, because we need to be able to determine the zeros of spherical Bessel functions for (potentially) large  $\ell$ . In particular, we need to determine an expression that describes the top surface in Fig. 4 for large  $k$  (the maximum value for  $\ell$  as a function of  $n$ , or vice versa). It turns out that  $\beta_{\ell,n}$ , the  $n$ th zero of the regular Bessel function of order  $\ell + \frac{1}{2}$ , satisfies the equality,<sup>29,37</sup>

$$\left(\ell + \frac{1}{2}\right) [\tan(\alpha) - \alpha] + \chi = n\pi \quad (\text{C.1})$$

(except possibly for  $n = 1$ ), where

$$\alpha \equiv \cos^{-1} \left( \frac{\ell + \frac{1}{2}}{\beta_{\ell,n}} \right), \quad (\text{C.2})$$

with  $0 \leq \alpha \leq \pi/2$ ; furthermore,  $\beta_{\ell,n} \geq \ell + \frac{1}{2}$ . The quantity  $\chi$  is defined as the phase of a particular integral along a contour in the complex plane (see Ref. 29) and is such that  $0 < \chi < \pi/4$ . For large zeros of Bessel functions,  $\chi$  approaches  $\pi/4$ ; that is, for fixed  $\ell$ ,<sup>29,38</sup>  $\lim_{\beta_{\ell,n} \rightarrow \infty} \chi = \frac{\pi}{4}$ . For large  $k$ , the relation between  $n$  and  $\ell$  on the integration boundary (that is, when  $\beta_{\ell,n} \simeq ka$ ) is given approximately by

$$n_{\text{sph}} = \frac{\left(\ell + \frac{1}{2}\right)}{\pi} [\tan(\alpha_{\text{sph}}) - \alpha_{\text{sph}}] + \frac{1}{4}, \quad (\text{C.3})$$

where

$$\alpha_{\text{sph}} \equiv \cos^{-1} \left( \frac{\ell + \frac{1}{2}}{ka} \right). \quad (\text{C.4})$$

Let us consider the lower limit for the integration in the  $n$  direction as well. The lower limit for the sum over  $n$  is  $n = 1$ . However, when approximating the sum by an integral, we need to be careful when all of the points lie exactly on the integration boundary (see the discussion between Eqs. (14) and (15)). Two options in this case are to extend the volume integral to the (unphysical) limit  $n = 1/2$ , which effectively captures all of the points having  $n = 1$ , or to keep the integration boundary at  $n = 1$ , but compute an area integral correction to make up for the fact that only half of the points at  $n = 1$  are captured in this case. Both

approaches give the same result to order  $k^2$ , so we choose the former approach.

It remains to determine the extreme upper limit for the integral over  $\ell$  (when  $n = 1$ ). To this end, we note the asymptotic expression,<sup>39</sup>

$$\beta_{\ell,1} \sim \left(\ell + \frac{1}{2}\right) + 1.8557571 \left(\ell + \frac{1}{2}\right)^{1/3} + \dots \quad (\text{C.5})$$

Thus, replacing  $\beta_{\ell,1}$  by  $ka$ , we see that when  $n = 1$ , the maximum value of  $\ell$  for large  $ka$  is approximately  $ka - 1/2$ . The integral is then<sup>40</sup>

$$N_{\text{sph}}(k) = \int_0^{ka-1/2} (2\ell + 1) \int_{\frac{1}{2}}^{n_{\text{sph}}} dn d\ell \quad (\text{C.6})$$

$$= 2 \int_0^{ka-1/2} \left(\ell + \frac{1}{2}\right) \left[ \frac{\left(\ell + \frac{1}{2}\right)}{\pi} [\tan(\alpha_{\text{sph}}) - \alpha_{\text{sph}}] + \frac{1}{4} - \frac{1}{2} \right] d\ell. \quad (\text{C.7})$$

For the terms involving  $\alpha_{\text{sph}}$ , we use Eq. (C.4) to perform a change of variables from  $\ell$  to  $\alpha_{\text{sph}}$  (noting that  $\alpha_{\text{sph}} \sim \pi/2 - 1/(2ka)$  when  $\ell = 0$  and  $ka$  is large). The resulting integrations are then readily performed, and we have

$$N_{\text{sph}}(k) = \frac{2(ka)^3}{9\pi} - \frac{1}{4}(ka)^2 + \dots \quad (\text{C.8})$$

$$= \frac{Vk^3}{6\pi^2} - \frac{Sk^2}{16\pi} + \dots \quad (\text{C.9})$$

which agrees with the expression in Eq. (8).

## 2. Circular cylinder

The integral approximation of  $N(k)$  is arguably more complicated in this case than in the previous two, although many of the considerations are similar to those we encountered for the spherical case. The integration boundary for  $n$  in terms of  $m$  and  $n_z$  is given by

$$n_{\text{cyl}} = \frac{m}{\pi} [\tan(\alpha_{\text{cyl}}) - \alpha_{\text{cyl}}] + \frac{1}{4}, \quad (\text{C.10})$$



where

$$\alpha_{\text{cyl}} \equiv \cos^{-1} \left( \frac{m}{a\sqrt{k^2 - \frac{\pi^2 n_z^2}{L^2}}} \right). \quad (\text{C.11})$$

The sum of states may be approximated by

$$N_{\text{cyl}}(k) = 2 \int_{\frac{1}{2}}^{n_{z,\text{max}}} \int_0^{m_{\text{bdy}}} \int_{\frac{1}{2}}^{n_{\text{cyl}}} dn \, dm \, dn_z \quad (\text{C.12})$$

$$= 2 \int_{\frac{1}{2}}^{n_{z,\text{max}}} \int_0^{m_{\text{bdy}}} \left[ \frac{m}{\pi} [\tan(\alpha_{\text{cyl}}) - \alpha_{\text{cyl}}] + \frac{1}{4} - \frac{1}{2} \right] dm \, dn_z, \quad (\text{C.13})$$

where  $m_{\text{bdy}}$  represents the large  $k$  limit of the boundary for  $m$  as a function of  $n_z$  when  $n = 1$ . The endpoint of the integration over  $n_z$  is slightly less than  $kL/\pi$  (the strict upper limit for the sum is  $(kL/\pi)\sqrt{1 - \zeta_{0,1}^2/(ka)^2}$ ).

To perform the integration over  $m$ , we use Eq. (C.11) to change variables to  $\alpha_{\text{cyl}}$ , noting that  $\alpha_{\text{cyl}} \rightarrow \pi/2$  as  $m \rightarrow 0$ . We denote the limit of  $\alpha_{\text{cyl}}$  as  $m \rightarrow m_{\text{bdy}}$  by  $\alpha_{\text{bdy}}$ , which satisfies the expression,

$$\sin(\alpha_{\text{bdy}}) - \alpha_{\text{bdy}} \cos(\alpha_{\text{bdy}}) = \frac{3\pi}{4} \frac{1}{a\sqrt{k^2 - \frac{\pi^2 n_z^2}{L^2}}}, \quad (\text{C.14})$$

leading to

$$N_{\text{cyl}}(k) \simeq \frac{k^3 a^2 L}{6\pi} - \frac{k^2 a^2}{8} + \frac{a^2}{4\pi} \int_{1/2}^{n_{z,\text{max}}} \left[ k^2 - \frac{\pi^2 n_z^2}{L^2} \right] \left[ -2\alpha_{\text{bdy}} \sin^2(\alpha_{\text{bdy}}) + \frac{5\pi \cos(\alpha_{\text{bdy}})}{2a\sqrt{k^2 - \frac{\pi^2 n_z^2}{L^2}}} \right] dn_z. \quad (\text{C.15})$$

It turns out that  $\alpha_{\text{bdy}}$  is small when  $k$  is large and  $n_z$  is not too close to  $kL/\pi$ . We expand the left-hand side of Eq. (C.14) for small  $\alpha_{\text{bdy}}$  to find

$$\alpha_{\text{bdy}}^3 \simeq \frac{9\pi}{4} \frac{1}{a\sqrt{k^2 - \frac{\pi^2 n_z^2}{L^2}}}, \quad (\text{C.16})$$

which allows us to estimate the order  $k^2$  terms in the remaining integral, leading to

$$N_{\text{cyl}}(k) = \frac{k^3 (\pi a^2 L)}{6\pi^2} - \frac{k^2 (2\pi a L + 2\pi a^2)}{16\pi} + \dots, \quad (\text{C.17})$$

in agreement with the first two terms in Eq. (8).

---

\* isaac\_bowser@taylor.edu

† knkiers@taylor.edu

‡ erica\_mitchell@taylor.edu

§ jokiers@live.unc.edu

- <sup>1</sup> H. P. Baltes and E. R. Hilf, *Spectra of finite systems: a review of Weyl's problem, The eigenvalue distribution of the wave equation for finite domains and its applications on the physics of small systems* (Mannheim, Wien, Zürich, Bibliographisches Institut, 1976).
- <sup>2</sup> F. Pockels, *Über die partielle differentialgleichung  $u + k^2y = 0$  und deren auftreten in der mathematischen physik* (Leipzig, Teubner Verlag, 1891).
- <sup>3</sup> J. Reudler, *Over de zwarte straling in ruimten van verschillende vorm*, doctoral dissertation (Leiden, 1912).
- <sup>4</sup> H. Weyl, “Über die asymptotische Verteilung der Eigenwerte,” *Göttingen Nachr.* 110–117 (1911);  
H. Weyl, “Das asymptotische Verteilungsgesetz der Eigenwerte linearer partieller Differentialgleichungen (mit einer Anwendung auf die Theorie der Hohlraumstrahlung),” *Math. Ann.* **71**, 441–479 (1912).
- <sup>5</sup> See Ref. 1, pp. 40–41 and pp. 54–56. Note the lengths to which early researchers had to go to accurately compute the zeros of Bessel functions (see pp. 38–39 in Ref. 1) – a task that can now be done easily using a high-level computer language such as *Mathematica*.
- <sup>6</sup> K.K. thanks H. Fisher for a thought-provoking conversation on this point.
- <sup>7</sup> M. I. Molina, “Ideal gas in a finite container,” *Am. J. Phys.* **64**(4), 503–505 (1996).
- <sup>8</sup> G. Gutiérrez and J. M. Yáñez, “Can an ideal gas feel the shape of its container?,” *Am. J. Phys.* **65**(8), 739–743 (1997).
- <sup>9</sup> R. K. Pathria, “An ideal quantum gas in a finite-sized container,” *Am. J. Phys.* **66**(12), 1080–1085 (1998).
- <sup>10</sup> S. J. Bereta, L. Madeira, V. S. Bagnato, and M. A. Caracanhas, “Bose-Einstein condensation in spherically symmetric traps,” *Am. J. Phys.* **87**(11), 924–934 (2019).
- <sup>11</sup> T. Price and R. H. Swendsen, “Numerical computation for teaching quantum statistics,” *Am. J. Phys.* **81**(11), 866–872 (2013).

- <sup>12</sup> D. Mulhall and M. J. Moelter, “Calculating and visualizing the density of states for simple quantum mechanical systems,” *Am. J. Phys.* **82**(7), 665–673 (2014).
- <sup>13</sup> The averaged asymptotic expression for  $N(k)$  [see Eq. (8)] is an expansion in powers of  $1/k$ , and ignores fluctuations arising from the discrete nature of the eigenvalues. In some cases these fluctuations are important as discussed in Ref. 14.
- <sup>14</sup> R. Balian and C. Bloch, “Distribution of eigenfrequencies for the wave equation in a finite domain: III. Eigenfrequency density oscillations,” *Ann. Phys.* **69**, 76–160 (1972).
- <sup>15</sup> W. N. Cottingham and D. A. Greenwood, *An Introduction to Nuclear Physics* (Cambridge University Press, Cambridge, 1986).
- <sup>16</sup> See, for example, D. Deutsch and P. Candelas, “Boundary effects in quantum field theory,” *Phys. Rev. D* **20**, 3063–3080 (1979), and also Ref. 17.
- <sup>17</sup> E. Elizalde and A. Romeo, “Essentials of the Casimir effect and its computation,” *Am. J. Phys.* **59**(8) 711–719 (1991).
- <sup>18</sup> See, for example, P. Harrison and A. Valavanis, *Quantum Wells, Wires and Dots: Theoretical and Computational Physics of Semiconductor Nanostructures*, 4th ed. (John Wiley, West Sussex, UK, 2016).
- <sup>19</sup> Some authors assign a factor of  $1/2$  for the equality condition and 1 for the less than condition [see Eq. (24)].<sup>1</sup> This modification becomes important for some of the higher-order terms in the expansion to be discussed, and we will adopt this prescription when it is important.
- <sup>20</sup> Daniel V. Schroeder, *An Introduction to Thermal Physics* (Addison Wesley Longman, San Francisco, 2000).
- <sup>21</sup> This expression is for bosons; an extra factor of two is usually included when considering a degenerate Fermi gas.<sup>20</sup>
- <sup>22</sup> R. Balian and C. Bloch, “Distribution of eigenfrequencies for the wave equation in a finite domain I. Three-dimensional problem with smooth boundary surface,” *Ann. Phys.* **60**, 401–447 (1970).
- <sup>23</sup> R. T. Waechter, “On hearing the shape of a drum: an extension to higher dimensions,” *Proc. Cambridge Philos. Soc.* **72**, 439–447 (1972).
- <sup>24</sup> See, for example, Refs. 8, 22, and 23. Results related to Eq. (8) are sometimes given in terms of the density of states (rather than the cumulative state number). Also, many of the formal results related to the distribution of eigenvalues of Eq. (1) are derived by solving related problems, such as the heat diffusion equation. See Ref. 22 for a discussion of this topic.

- <sup>25</sup> See Ref. 1 for a similar expression for the cubic case.
- <sup>26</sup> For a complementary description, we refer interested readers to Ref. 12.
- <sup>27</sup> See, for example, P. R. Bevington and D. K. Robinson, *Data Reduction and Error Analysis for the Physical Sciences*, 3rd ed. (McGraw-Hill, New York, 2003).
- <sup>28</sup> Kim, H. *et al.* “Quasi-one-dimensional density of states in a single quantum ring,” *Sci. Rep.* **7**, 40026 (2017).
- <sup>29</sup> G. N. Watson, “The zeros of Bessel functions,” *Proc. Royal Soc. XCIV. A* **94**, 190–206 (1918).
- <sup>30</sup> R. H. Lambert, “Density of states in a sphere and cylinder,” *Am. J. Phys.* **36**(5), 417–420 (1968).
- <sup>31</sup> We can also use embedded Do loops; it is tricky to determine the upper limits for each of the loops.
- <sup>32</sup> It is possible to miss degeneracies due to rounding or other issues, which can be checked after the fact by comparing subsequent  $\kappa$  values to determine if they are very close to each other.
- <sup>33</sup> See, for example, M. L. Boas, *Mathematical Methods in the Physical Sciences*, 3rd ed. (John Wiley & Sons, Inc., Hoboken, 2006).
- <sup>34</sup> SciPy Cookbook, *Spherical Bessel Zeros*, <<https://scipy-cookbook.readthedocs.io/items/SphericalBesselZeros.html>>.
- <sup>35</sup> More mathematically sophisticated approaches, which correctly account for the averaging procedure, are described in Refs. 1, 8, 22, and 23. We agree with Lambert that, “As an alternative to the rather inaccessible general proof, it seems worthwhile to give explicit proofs for the sphere and the cylinder since these shapes. . . will tend to make the general result more plausible.”<sup>30</sup> Reference 22 gives a beautiful introduction to a method involving the diffusion equation, Green’s functions and a Laplace transform.
- <sup>36</sup> See also Ref. 3 for an early calculation of the volume term for the spherical and cylindrical cases in the context of blackbody radiation.
- <sup>37</sup> G. N. Watson, *A Treatise on the Theory of Bessel Functions*, 2nd ed. (The Syndics of the Cambridge University Press, London, 1966).
- <sup>38</sup> We have used Eqs. (C.1) and (C.2) to determine  $\chi$  near the boundary. The largest deviation occurs for  $n = 1$ , for which  $\chi \sim 0.965 \times \pi/4$  for large values of  $\beta_{\ell,1}$  (a result that can be derived using Eq. (C.5)).
- <sup>39</sup> M. Abramowitz and I. A. Stegun, *Handbook of Mathematical Functions with Formulas, Graphs and Mathematical Tables* (Dover Publications, New York, 1965), Eq. (9.5.14).

<sup>40</sup> One might wonder whether a correction is required for the points with  $\ell = 0$ . These points form a line in  $n$ - $m$ - $\ell$  space, so the corresponding correction would be of order  $k$ . Note that we have inserted the degeneracy factor of  $2\ell + 1$  as a sum in the first line of Eq. (C.7), rather than as an integral. If we had done the integral from  $-\ell$  to  $\ell$  instead, we would have obtained  $2\ell$  instead of  $2\ell + 1$ , which would have yielded the same result at order  $k^3$ , but would have differed at order  $k^2$ . The reason for the difference is that the bounding surfaces suspended above the  $n$ - $m$  plane (see Fig. 4) contain the points with  $m = \pm\ell$ , and these points all lie precisely on these surfaces. If we had done the integral in the  $m$  direction, we would only have captured half of the points on these surfaces (see the discussion between Eqs. (14) and (15) in Sec. II A). To correctly capture all of these points, we can extend the range of the integration to be between  $-\ell - 1/2$  to  $\ell + 1/2$ , which gives the same result as the sum.